BNL-216124-2020-JAAM

A highly stable Cu(OH)(2)-Poly(vinyl alcohol) nanocomposite membrane for dramatically enhanced direct borohydride fuel cell performance

W. Chu, Y. S. Chu

To be published in "JOURNAL OF POWER SOURCES"

August 2020

Photon Sciences

Brookhaven National Laboratory

U.S. Department of Energy

USDOE Office of Science (SC), Basic Energy Sciences (BES) (SC-22)

DISCLAIMER

A highly stable $Cu(OH)_2$-Poly(vinyl alcohol) nanocomposite membrane for dramatically enhanced direct borohydride fuel cell performance

Wen Chu[a], Yan He[b], Yong S. Chu[d], Liang Meng[a], Jiabin Liu[a*], Haiying Qin[c*], Shanwen Tao[e*]

[a] School of Materials Science and Engineering, Zhejiang University, Hangzhou 310027, P. R. China.

[b] Shanghai Synchrotron Radiation Facility, Shanghai Institute of Applied Physics, Chinese Academy of Sciences, Shanghai, 201800, P. R. China

[c] College of Materials and Environmental Engineering, Hangzhou Dianzi University, Hangzhou 310018, P. R. China.

[d] National Synchrotron Light Source II, Brookhaven National Laboratory, Upton, New York 11973, USA.

[e] School of Engineering, University of Warwick, Coventry, CV4 7AL, UK

Abstract:

Nano-additive aggregation, limited performance, and unclear modification mechanisms are the main obstacles in developing nanocomposite anion exchange membranes (AEMs). In this work, for the first time, an effective and highly stable Poly(vinyl alcohol) (PVA)-based AEMs with dispersive $Cu(OH)_2$ nanoclusters (Cu-AEMs) are prepared by a simple and eco-friendly three-step method: '$CuCl_2$ doping-casting-KOH immersing'. The doped Cu^{2+} ions chemically combine with OH^- ions to form anionic conductive $Cu(OH)_2$ nanoclusters intermediated by attaching resins. The PVA skeletons wrap around $Cu(OH)_2$ while the hydroxyl groups are exposed to bulk water, forming $Cu(OH)_2$-PVA complex, which avoids nano-additive aggregation, increases anionic channels, and strengthens additive-matrix connection. A direct borohydride fuel cell using Cu-AEM with 0.56 wt. % $CuCl_2$ possesses the highest power density of 403.3 $mW \cdot cm^{-2}$ at 60 °C and a life span of over 200 h. The high-performance and durability come from the unique structure of $Cu(OH)_2$ nanoclusters-PVA complex. 'Vehicle' theory is considered to be the dominant mechanism for enhancing such nanocomposite Cu-AEMs. This work demonstrates a

* Corresponding author.
Tel: +86-571-87951027; Fax: +86-571-87951027
E-mail address: liujiabin@zju.edu.cn (Jiabin Liu), hyqin@hdu.edu.cn (Haiying Qin) and S.Tao.1@warwick.ac.uk (Shangwen Tao)

new concept for preparing the stable AEMs toward high-performance fuel cells. The synthetic chemistry involved can be broadly extended for fabricating versatile AEMs.

Key-words: Direct borohydride fuel cells; Anion exchange membranes; Nanocomposites; Poly(vinyl alcohol); Copper hydroxide

1. Introduction

Direct borohydride fuel cell (DBFC) is a promising future power source for its low operating temperature, convenient transportation, and possible use of nonprecious metals catalysts [1-5]. Anion exchange membrane (AEM) with separating and conducting functions is a key component of DBFCs [6]. Recently, the rapidly enhanced anionic conductivity of AEMs, which even exceeds that of proton exchange membranes, is attracting more attention [5-8]. The state-of-art AEMs are mainly obtained through chemical modifications on quaternary ammonium type electrolytes and have some key issues such as water management, chemical instability, and high cost [9-11]. Nanocomposites that take advantage of the large specific surface area of nano-materials and combine the properties of organics and inorganics show excellent potential in solving these problems in the last decade [6, 10, 11]. For instance, the poly(arylene ether sulfone)/nano-ZrO_2 AEM used in alkaline fuel cells (FCs) exhibits improved water uptake, hydroxide conductivity, and stability [12, 13]. But there are still some uncovered issues in nanocomposite AEMs comparing with commercial AEMs, e.g., nanofiller aggregation, weak additive-polymer connection, and limited properties [9, 14-17]. The aggregation behavior of nano-additives is related to the type, size, shape, and concentration of additive, the pH value of solvent, and the preparation [18-23]. The nano-additives, including modified carbon nano-materials, graphene-based nanomaterials, and metal oxides, have been introduced into AEMs by traditional sol-gel and alkali soaking method [13-15, 24-26]. The *in-situ* interfacial synthesis method is proposed recently to relieve the aggregation of nano-additives, in which nano-additives are synthesized by the phase transformation of precursors with specific solvent and assistants [13-15, 24]. Some assistants are also used to strengthen the additive-polymer connection in composites [27]. Great prospects can be expected if more high-performance and stable nanocomposite AEMs can be prepared without any assistance [14-17, 21]. Although the good compatibility with the alkaline

environment, only a few metal hydroxides such as nanosized $Mg(OH)_2$ are added into AEMs through a sol-gel method [28]. PVA-based CoO(OH) composite AEMs with low permeability and high-performance have been prepared by adding CoO(OH) catalysts in membranes to accelerate the decomposition of permeated fuel [29]. After extensive research, we found that Cu^{2+} ions in the PVA gel at pH > 6 will transform to dispersive $Cu(OH)_2$ nanoclusters by reacting with free OH^- in water, which is similar to the *in-situ* synthesis process [30, 31]. Nano-sized $Cu(OH)_2$ is an assembly of insoluble clusters (flowers) that have exhibited significant applying potential as photo-catalyst and supercapacitor materials in alkaline media [32, 33]. PVA is a water-soluble polymer and a strong candidate for anion exchange applications with good charge storage capacity, good ionic conductivity, and low cost [34]. $Cu(OH)_2$ has the potential of modifying PVA-based AEMs. On the one hand, $Cu(OH)_2$ can adsorb OH^- ions and transform to $[Cu(OH)_4]^{2-}$ in lye, which indicates its potential as the anionic conductors [35]. On the other hand, hydrophobic interactions make $Cu(OH)_2$ particles soluble in aqueous polyhydric alcohols (such as PVA) [36, 37]. The hydrophobic PVA skeletons encapsulate the $Cu(OH)_2$ to form core-shell complex while the hydrophilic hydroxyl groups on PVA chains orient toward the bulk water, resulting in separate hydrophobic and hydrophilic domains [36, 38]. Besides, the modification mechanisms of advanced nanocomposite AEMs are still unclear [39, 40]. Some studies believe the reduced permeation or the increased electron-carriers is the key, while others believe the enhanced ratio of conductivity to permeability is the reason for the improved performance of nanocomposites [7, 8, 40].

Herein, we achieved the *in-situ* synthesis of dispersive $Cu(OH)_2$ nanoclusters in the PVA matrix through a simple and green "$CuCl_2$ doping-casting-KOH immersing" method. What we developed not only avoids the aggregation of nano-additives but also increases the number and size of anionic channels. The dominant enhanced mechanism of such nanocomposite AEMs is systemically investigated.

2. Experimental

2.1. Materials

Polyvinyl alcohol (PVA, MW 57000-66000), anion exchange resin (AER, Amberlite IRA-402, hydroxide form), $CuCl_2 \cdot 6H_2O$, KOH, and NaOH for membranes preparation were supplied by Alfa Aesar. The AER with positive charged quaternary

ammonium groups can be applied as anion conductor in energy devices. The AER was ground with an agate mortar and sifted by a 200 mesh sieve before use.

2.2. Preparation of the membranes

The nanocomposite AEMs were prepared from $CuCl_2 \cdot 6H_2O$, AER, and PVA (denotes as Cu-AEMs in the following). The mass fractions of $CuCl_2 \cdot 6H_2O$ in AEMs were set as 0, 0.14, 0.56, 1, and 1.4 wt. %, respectively. For instance, adding 0.14g $CuCl_2 \cdot 6H_2O$ into the gel with 33.29 g AER, 66.57 g PVA, and 466 mL de-ionized water to prepare Cu-AEMs with 0.14 wt. % $CuCl_2 \cdot 6H_2O$.

The preparation of Cu-AEMs can be divided into the following three steps:

I. Adding certain content of $CuCl_2 \cdot 6H_2O$ into PVA aqueous to get gel A.
II. Adding AER into $CuCl_2$-PVA gel (gel B), casting and drying of the gel B.
III. Immersing $CuCl_2$-PVA-AER AEMs into 1 M KOH for 24 h.

A flow chart of the Cu-AEMs preparation process with three steps is provided in supplementary as Fig. S1. In step I, $CuCl_2$ and PVA were stirred and dissolved in de-ionized water at 95°C for 2 h to get a series of $CuCl_2$-PVA gels (gel A). The gel A was still stood at 50 °C for 15 min to avoid the activity decline of AER and to remove bubbles. Then in step II, the gel A was mixed thoroughly with prepared AER powder to get gel B. The wet gel B was cast on a glass plate and dried naturally at room temperature for 48h to form PVA-AER membranes impregnated with Cu^{2+} ions (Cu-AEMs). The thickness of gel B on the plate was controlled at 1 mm, and the thickness of dry Cu-AEMs was ~ 200 μm. In step III, Cu-AEMs were immersed in 1 M KOH solution for 24 h before being used in DBFCs (denoting as blank Cu-AEM, 0.14%Cu-AEM, 0.56%Cu-AEM, 1%Cu-AEM, and 1.4%Cu-AEM in the following text). The thickness of dry Cu-AEMs can be adjusted base on needs from 50 to 500 μm by controlling the thickness of wet gel B. The Cu-AEMs used in cell performance tests and lifetime tests were ~120 μm (wet AEMs are ~150 μm) in thickness.

2.3. The chemical changes in Cu-AEMs

The photographs of reactions between $CuCl_2$, PVA, and AER were taken to illustrate the chemical changes during the preparation. Furthermore, maping of Cu elemental distribution was carried out to clearly show the changing process of additive. High resolution mapping of Cu distribution in in Cu-AEMs samples, via

nanoscale X-ray fluorescence imaging, was conducted at the Hard X-ray Nanoprobe (HXN) Beamline at National Synchrotron Light Source II (NSLS-II) of the Brookhaven National Laboratory. The monochromatic X-rays at 9 keV were focused using a Fresnel X-ray zoneplate to produce an 80 nm × 80 nm spot. The fluorescence imaging measurements were conducted by scanning the sample with a continuous fly-scan mode and by collecting the emitted fluorescence X-rays using a three-element silicon drift detector (Vortex 3ME). Element distribution images were obtained by fitting the scanning fluorescence spectra using an X-ray fluorescence analysis software PyXRF.

2.4. Membrane characterizations

Differential scanning calorimetry-thermogravimetric analysis (DSC-TGA) was carried out on SDT Q600 to detect the thermal stability of Cu-AEMs. The measurements were conducted by heating samples from 30 to 600 ^{o}C at a rate of 5 ^{o}C·min^{-1} in flowing nitrogen at a rate of 120 mL·min^{-1}. The crystal structure of Cu-AEMs was carried on a Philips X' PERT-PRO X-ray diffractometer. The valence of the copper element was identified by the X-ray absorption near edge structure (XANES) measured in BL15U1 at the Shanghai Synchrotron Radiation Facility (SSRF). To get the swelling ratios (*SR*), the dimensions of dry Cu-AEMs were measured at first (denotes as L_{dry}). Then Cu-AEMs were immersed in de-ionized water at 25 °C for 48 h and wiped with lens paper. The dimensions of immersed Cu-AEMs were determined again as L_{wet}. The *SR* was calculated by equation (1) [41]:

$$SR = (L_{wet} - L_{dry})/L_{dry} \quad (1)$$

The size of ionic channels in wet Cu-AEMs was measured by an Xsnocs small angle X-ray scattering system (SAXS) operating at 50 kV and 0.6 mA for 1200 s. The radiation used in SAXS test was 0.15148 nm, and the working distance was 185 mm.

2.5. Hydroxide conductivity

The anionic conductivity tests were measured at 25 ^{o}C under 100% humidity using an electrochemical station (Gamry interface 1000, USA). The resistances of AEMs were measured through a two-probe AC-impedance test with a frequency range of 1 MHz to 1 Hz at a bias of 5 mV. To get the real anionic conductivity, Cu-AEMs were assembled into cells with carbon papers as electrodes and fuel of

DBFCs as a testing solution. The conductivity (σ) was calculated by equation (2) [42]:

$$\sigma = t/RA \quad (2)$$

where t is the membrane thickness, A is the active area of the membrane, and R is the resistance of the membrane measured by a.c. impedance.

Since the anionic conductivity of Cu-AEM includes the conduction of Cu^{2+}, OH^-, and electrons, the hydroxide conductivity should be the difference between anionic conductivity and conductivities of Cu^{2+} and electrons. The resistances of Cu-AEM in a cell using Cu foil as electrodes were also measured to reflect the conductivity of Cu^{2+} ions and electrons.

2.6. Fuel permeability

Fuel permeabilities of Cu-AEMs under the electric field were measured using a three-chamber device with a permeating chamber and two receiving chambers. There were 3 cm × 4 cm openings covering with silver meshes at one side of receiving chambers and both sides of the permeating chamber. The Cu-AEMs were clamped by the receiving chamber and permeating chamber, and the whole device was sealed by O-rings. Before the test, a voltage was applied to the silver meshes to simulate the internal electric field in real cells.

The permeability test is based on the sensitivity of the nicotinamide adenine dinucleotide-tris (hydroxymethyl) aminomethane buffer solution (NAD-tris**)** to BH_4^- ions. The concentration of BH_4^- ions in the receiving chamber was calculated by the absorbance of a liquid sample and the Abs-BH_4^- concentration standard curve *via* a UV-Vis spectrophotometer (Agilent Cary 5000). The change rate of BH_4^- concentration in the receiving chamber with time was used as an evaluation index of the fuel permeability. The permeabilities of Cu-AEMs were calculated according to the following equation [43]:

$$P = (\text{slope})\frac{lV}{CS} \quad (3)$$

where the slope is the slope of the concentration-time line, V is the volume of liquid in each receiving chamber, C was the initial BH_4^- concentration in permeating chamber, and S was the opening area for BH_4^- permeating. More detailed procedures and device illustrations of the permeability tests have been published in previous work [44].

2.7. Fuel cell performance

The cell performance of DBFCs using Cu-AEMs was evaluated at 30 °C and 60 °C, respectively, by a PFX-2011 battery test system (Kikusui Electronics Corp). The humidified O_2 with a flow rate of 100 mL·min^{-1} was fed into the cathode under a pressure of 0.2 MPa. An alkaline $NaBH_4$ solution (containing 5 wt. % $NaBH_4$ and 10 wt. % NaOH) was fed into cells as fuel with a flow rate of 10 mL·min^{-1}. The cell using Cu-AEMs had a working area of 6 cm^2 and employed polypyrrole modified carbon-supported cobalt hydroxide ($Co(OH)_2$-PPy-BP) as the catalysts for both anode and cathode. The preparation of $Co(OH)_2$-PPy-BP is described in the previous report [43]. The lifetime of a DBFC using 0.56%Cu-AEM was tested to evaluate the stability of Cu-AEMs. The cell was discharged at 30 ºC with a current density of 50 mA·cm^{-2}, and its voltage was recorded every hour. The working area, O_2 pressure, fuel flow rate, catalysts, and other parameters of lifetime tests were the same as those of cell performance tests.

3. Results and discussion

3.1. The interactions among the components

In Fig. 1a-b, $CuCl_2·6H_2O$ and AER were dispersed in DI water, forming a uniform solution and a suspension, respectively. Figure 1c shows a homogeneous gel of $CuCl_2$ and PVA. Figure 1d shows the obvious agglomerations that occurred in an AER-PVA mixture with 2 wt. % $CuCl_2$, indicating that Cu^{2+} ions prefer to adhere to AER than to PVA and too many Cu^{2+} ions will aggregate around AER. The cyan floc in Fig. 1e is believed to be the self-assembly of Cu^{2+} ions on the AER surface, which is supported by previous work (Fig. 1g) [8]. Hybrid AERs doping with various Cu-based salts have been applied in separation, purification, and ionic selection [45-48]. Figure 1e-f are images of $CuCl_2$-AER-PVA gels with a higher content of Cu^{2+} (5 times of 0.56%Cu-AEM) and lower content of PVA (20% of 0.56%Cu-AEM) before and after alkali immersing. The blue colored complex in Fig. 1e transformed into dark-colored precipitation after alkali immersing. The XRD patterns of Fig. 1h corresponds to the naturally dried gels of Fig. 1e-f, which is used to elucidate the composition of Cu element in Cu-AEMs. The diffraction peak at ~16.5, 33.5, and 40 º are detected in $CuCl_2$-PVA-AER gels and peaks at ~17, 24, 35, 40, and 53 º appear

after alkali immersion. These peaks accurately match with those of $Cu_2Cl(OH)_3$ and $Cu(OH)_2$ in JCPDS database (PDF #50-1559 and #13-0420), respectively. These analyses indicate that Cu^{2+} ions in Cu-AEMs exist in the form of hydroxide throughout the whole preparation. The Cu^{2+} ions in Cu-AEMs firstly convert to PVA wrapped $Cu(OH)_2$ complex in a neutral PVA gel by combining with free OH^- ions in water, which has been applied in preparing core-shell medicines and nano Cu [30, 31]. Then the $Cu(OH)_2$-PVA complex chemically combine with OH^- ions, forming dispersive $Cu(OH)_2$ nanoclusters.

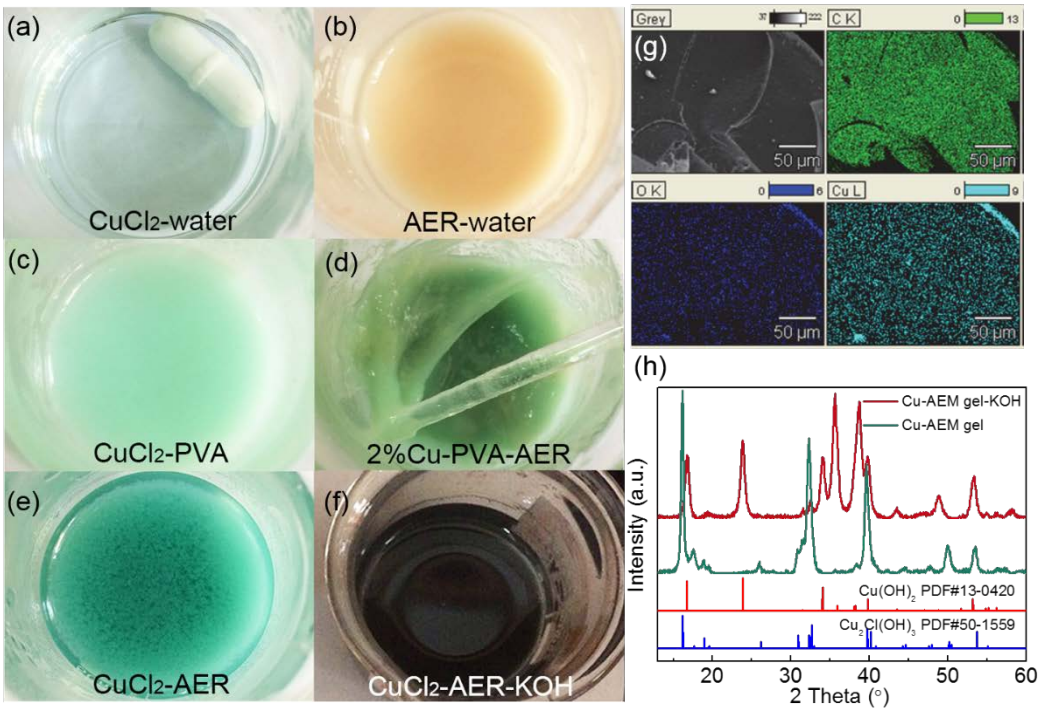

Fig. 1. The reactions between different components: (a) $CuCl_2$-water, (b) AER-water, (c) 0.56 wt. % $CuCl_2$-PVA, (d) 2%Cu-AER-PVA gel; digital photos of (e) $CuCl_2$-AER-PVA gel with 500 % Cu^{2+} and 20 % PVA comparing with 0.56%Cu-AEM, (f) KOH solution immersed $CuCl_2$-AER-PVA gel in (e), (g) the SEM image with EDS mapping on the cross-section of the Cu^{2+} doped resins in ref. [8], and (h) the XRD results of $CuCl_2$-AER-PVA gel before and after KOH immersing (corresponding to Fig. 1 e and f).

3.2. The Cu element distribution

The change of Cu element distribution in Cu-AEMs during preparation was studied using high spatial resolution X-ray fluorescence imaging. In Fig. 2a-b, the micron-sized Cu enrichments form through the combination of $Cu(OH)_2$-PVA complex and AER (denoting as $Cu(OH)_2$-AER particles). As $CuCl_2$ increase from

0.54 to 1.4 wt. %, the $Cu(OH)_2$-AER particles enlarge and agglomerate. These micro-sized $Cu(OH)_2$-AER particles in Cu-AEMs transform into dispersive $Cu(OH)_2$ nanoclusters after alkali immersing, as suggested in Fig. 2c-d. The background color of Fig. 2dnoticeably changed, indicating the overwhelming of $Cu(OH)_2$ nanoclusters in 1.4%Cu-AEM.

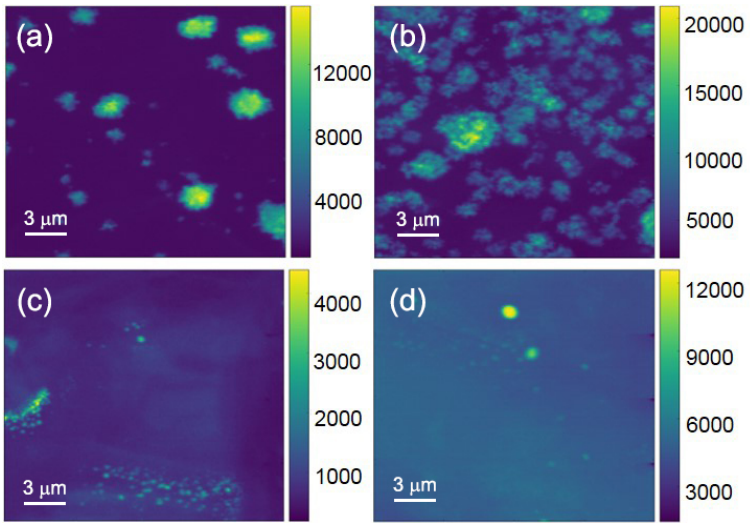

Fig. 2. The distribution of copper element in Cu-AEMs: (a) 0.56%Cu-AEM, (b) 1.4%Cu-AEM, (c) KOH soaked 0.56%Cu-AEM, and (d) KOH soaked 1.4%Cu-AEM.

3.3. The microstructural changes in Cu-AEMs

The schematic microstructures of Cu-AEMs are vividly shown in Fig. 3a-c and the number and size of $Cu(OH)_2$-AER particles increase with the increase of Cu^{2+}. In blank Cu-AEM (Fig. 3a), PVA chains interweave into a membrane, and AER powders imbed into the gap among PVA chains. In 0.56%Cu-AEM (Fig. 3b), the $Cu(OH)_2$-PVA complex adheres to AER, forming micro-sized particles. The $Cu(OH)_2$-AER particles aggregated and interrupted the polymers' interweaving in 1.4%Cu-AEM (Fig. 3c).

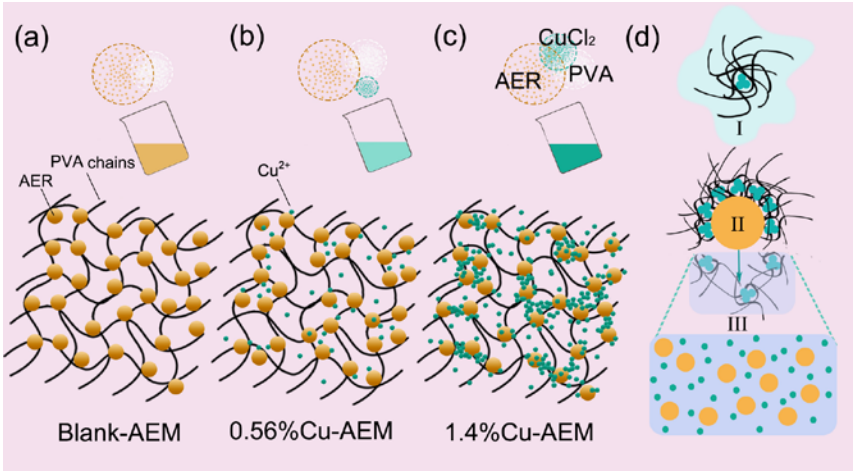

Fig. 3. The schematic diagrams of microstructures of (a) blank Cu-AEM, (b) 0.56%Cu-AEM, and (c) 1.4%Cu-AEM; (d) the chemical and positional changes of Cu^{2+} in Cu-AEMs during preparation.

The preparation of Cu-AEMs has three steps: I, adding Cu^{2+} into PVA gel; II, adding AER into Cu^{2+}-PVA gel, casting and drying; III, KOH immersing. The chemical and positional changes of Cu^{2+} in Cu-AEMs during preparation are shown in Fig. 3d. In step I, different contents of $CuCl_2$ are added into PVA gels. As mentioned earlier, the Cu^{2+} in a neutral PVA gel will transform to $Cu(OH)_2$-PVA complex. The hydroxyl groups on the PVA chains oriented toward bulk water while the hydrophobic skeletons encapsulate the $Cu(OH)_2$ particles, making the $Cu(OH)_2$-PVA complex soluble [36, 38]. In step II, the soluble $Cu(OH)_2$-PVA complex attaches to the surface of AER, forming $Cu(OH)_2$-AER core-shell particles. In step III, dry Cu-AEMs are immersed into 1 M KOH, and the $Cu(OH)_2$-PVA complex detaches from AER and converts into dispersive $Cu(OH)_2$ nanoclusters. The agglomeration of nanofillers is a challenging topic in nanocomposites [22, 49]. The *in-situ* synthesis method is a novel way to avoid the agglomeration of nanofillers by the phase transition from soluble precursors to dispersive nanofillers in certain conditions [50, 51]. During the preparation of Cu-AEMs, three major components in Cu-AEMs (i.e. PVA, AER, and OH^- ions) combine with Cu^{2+} in turn, because their binding forces with Cu^{2+} are stronger one by one. The different binding energies between the three components and Cu^{2+} is the underlying reason for the *in-situ* synthesis of $Cu(OH)_2$ nanoclusters. The phase transition from $Cu(OH)_2$-AER particles to dispersive $Cu(OH)_2$ nanoclusters achieves *in-situ* nano-additive synthesis in a simple and green way. The stronger connection between PVA and $Cu(OH)_2$ nanoclusters is also

beneficial to the stability of Cu-AEMs [22]. Besides, the surface of $Cu(OH)_2$ nanoclusters is capable of absorbing OH^-, which increases anionic channels and improves the properties of AEMs [35].

3.4. Membrane properties

As shown in Fig. 4a, all the tested Cu-AEMs have three stages of weight loss in TGA tests. Stage I corresponds to the removal of free water inside of membranes. Stages II and III correspond to the breaking down of PVA chains and the decomposition of amino groups, respectively [52, 53]. The quantified weight losses of each stage are presented in Fig. 4b. The $CuCl_2$ modified AEMs has less weight loss in stages II, III, and higher residual weight than the blank AEM.

The enthalpy values in Fig. 4d were calculated by the areas of DSC peaks at ~230 and 420 °C in Fig. 4c to evaluate the crystallinities of Cu-AEMs. The measured enthalpy at peak 1 of the blank Cu-AEM (331.61 $mJ \cdot g^{-1}$) is higher than that of other Cu-AEMs (~280 $mJ \cdot g^{-1}$), showing the crystallinity decrease of $Cu(OH)_2$ nanocomposites [54].

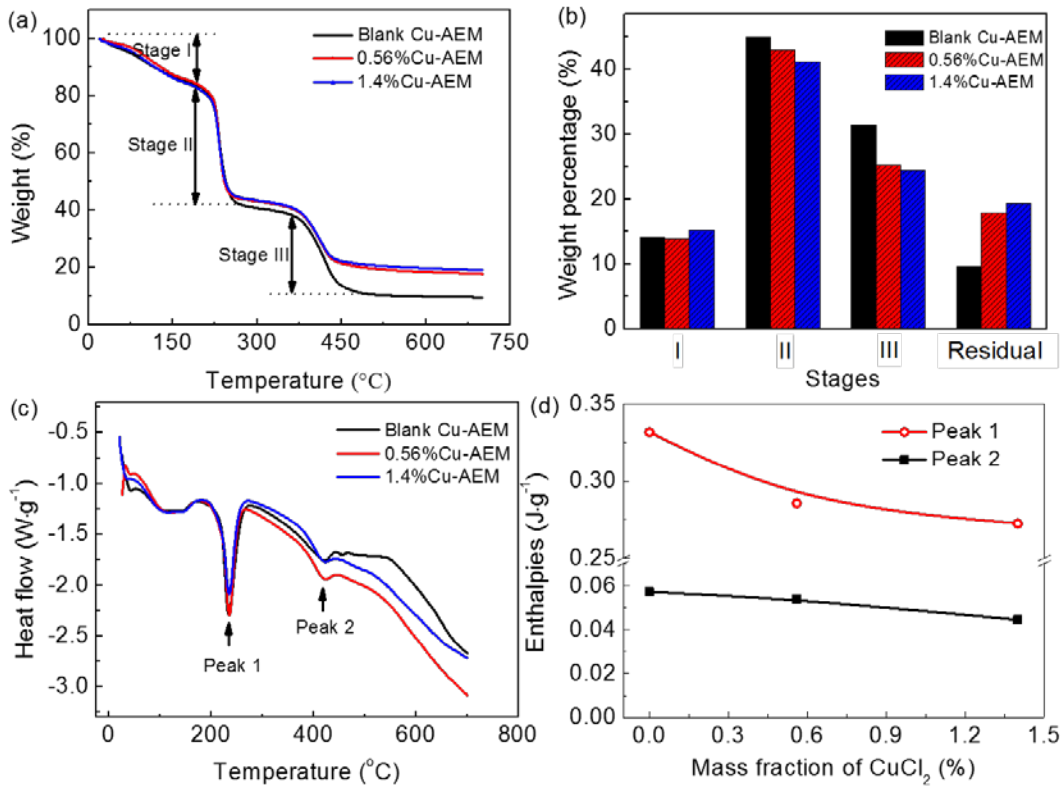

Fig. 4. (a) The TGA results of Cu-AEMs and (b) quantified weight losses of decomposition stages

in TGA results; (c) DSC results of Cu-AEMs and (d) the enthalpies of exothermic peaks in DSC results.

The XRD spectra of Cu-AEMs are presented in Fig. 5a. Two diffraction peaks at 19.5 and 40.1 ° are the crystalline peaks of crystalline phase PVA, and no other peak is observed due to the large amount of PVA in Cu-AEMs [55]. Therefore, we tested the XRD spectra of dried $CuCl_2$-PVA-AER gels with less PVA and more $CuCl_2$ to confirm the existence of $Cu(OH)_2$ nanoclusters (Fig. 2). The similarity between Cu K-edge XANES results of 1.4%Cu-AEM and $Cu(OH)_2$ in Fig. 5b confirms? that the valence of Cu element in the synthesized Cu-AEMs should be +2 [56]. As shown in Fig. 5c, the swelling degree of Cu-AEMs firstly increase and then decrease as the $CuCl_2$ content increase from 0 to 0.56 and1.4 wt.%. The unexpected high *SD* results from the better contact between hydroxyl groups on PVA chains and water molecules in $Cu(OH)_2$ nanocomposites. The SAXS results in Fig. 5d reflect the change of anionic channels in Cu-AEMs. A distinct SAXS peak occurs at 11.8 nm^{-1} in 1.4%Cu-AEM, indicating the enlargement of anionic channels [57]. The $Cu(OH)_2$ nanoconductors, as well as the separating hydrophobic and hydroxyl regions in Cu-AEMs, explain the expanding of anionic channels.

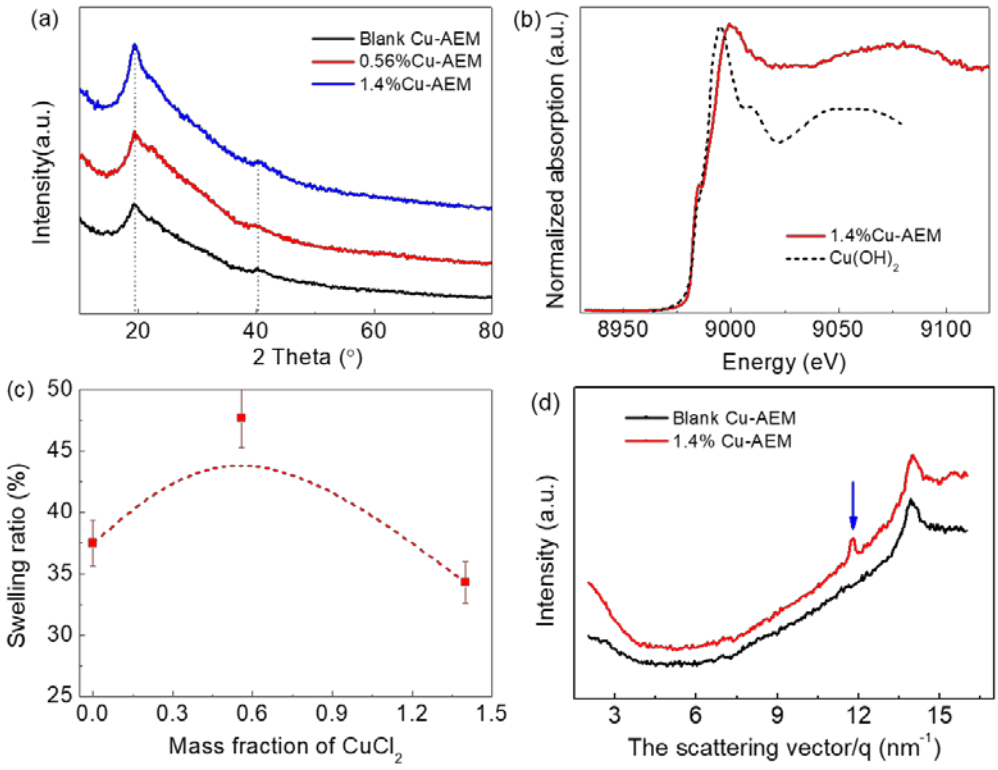

Fig. 5. (a) The XRD results of Cu-AEMs, (b) the XANES spectra of 1.4%Cu-AEM and reported

$Cu(OH)_2$ [56], (c) the swell degree of Cu-AEMs, (d) the SAXS results of blank Cu-AEM and 1.4%Cu-AEM.

3.5. Conductivity and permeability

The movable charged-species within Cu-AEMs include OH^-, Cu^{2+}, and electrons. The resistances of FCs using Cu-AEMs as electrolytes and carbon papers or Cu foils as electrodes were measured separately to get the hydroxide conductivity. As shown in Fig. 6a, the Cu^{2+} and electrons conductivity of 0.56%Cu-AEM (5.56×10^{-5} $S\cdot cm^{-1}$) is negligible compared to its total anionic conductivity (2.8×10^{-2} $S\cdot cm^{-1}$), which means most of the conducting anions in Cu-AEMs are OH^- ions. The anionic conductivity and permeability of Cu-AEMs exhibit similar trends that increase as the $CuCl_2$ content increase from 0 to 0.56 wt. % and decrease at 1.4 wt. %. It is because both the fuel (BH_4^-) and OH^- in DBFCs can across AEMs freely. 0.56%Cu-AEM has both the highest conductivity of 2.8×10^{-2} $S\cdot cm^{-1}$ and the highest permeability of 2.94×10^{-6} $s^{-1}\cdot cm^2$.

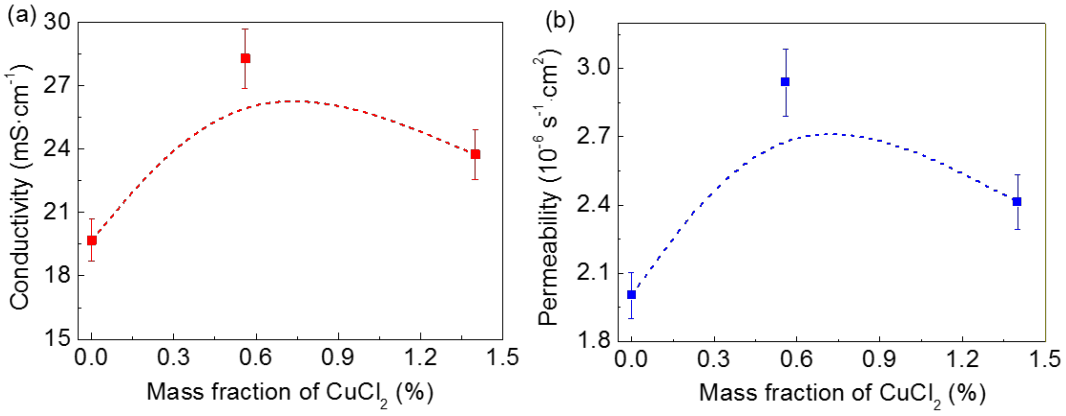

Fig. 6. The (a) anionic conductivity and (b) fuel (BH_4^-) permeability of Cu-AEMs.

3.6. Fuel cell performance

The cell performance of DBFCs using Cu-AEMs (Fig. 7) is a comprehensive indicator to study the modification mechanisms of nanocomposites [58]. Figures 7a-e are the cell voltage (*U*) and power density (*P*) of DBFCs using Cu-AEMs. All the voltages decrease with the increase of discharging current density. The power densities of DBFCs continuously increase with current density until reaching the maximum voltage of ~ 0.5 V. The power densities of the DBFCs tested at 60 °C are notably higher than those at 30 °C. The maximum power densities (P_{max}) of DBFCs

are summarized in Fig. 7f and the DBFC using 0.56%Cu-AEM achieves the highest P_{max} of 215.51 and 403.26 mW·cm^{-2} at 30 °C and 60 °C, respectively.

The open cell voltages of DBFCs using Cu-AEMs (red arrows in Fig. 7) are unaffected, suggesting the amount of permeating BH_4^- ions in Cu-AEMs is low despite the high permeabilities. Electrochemical impedance spectroscopy (EIS) was also used to evaluate the resistances of ions transfer through Cu-AEMs and interfaces (including the diffusion boundary layer and the electrical double layer) [59-61]. As shown in Fig. S2, the R_{ohm}, R_a, and R_c of DBFC using 0.56%Cu-AEM is lower than the DBFCs using other Cu-AEMs. Since the EIS results mainly reflect the conducting ability of AEMs, the lower resistances of 0.56%Cu-AEM prove that anionic conductivity is a decisive factor in the performance of nanocomposites.

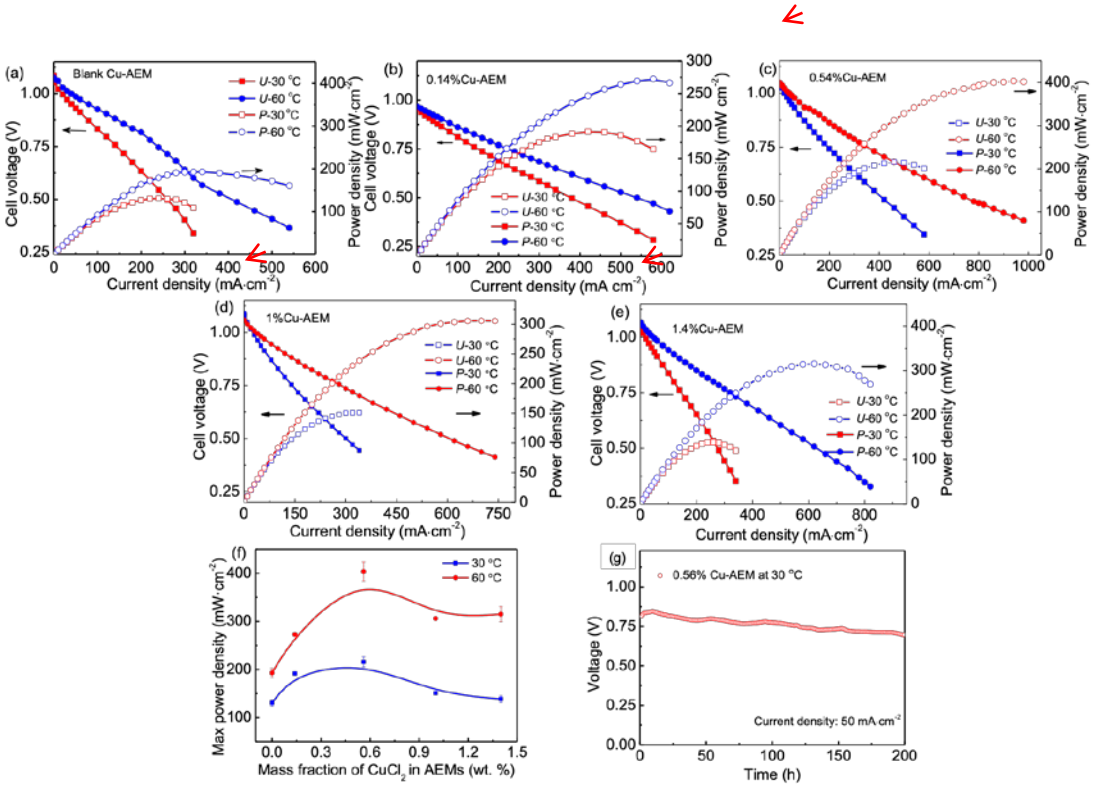

Fig. 7. The cell performance of DBFCs using (a) blank Cu-AEM, (b) 0.14%Cu-AEM, (c) 0.56%Cu-AEM, (d) 1%Cu-AEM, and (e) 1.4 %Cu-AEM; (f) the P_{max} of DBFCs using Cu-AEMs with different content of $CuCl_2$; (g) the lifetime test of a DBFC using 0.56%Cu-AEM at 30 °C with a current density of 50 mA·cm^{-2}.

Excellent stability is a prerequisite for the development of the fuel cell industry [6]. Therefore, the usually used additives in electrolytes are stable materials such as silicon dioxide, titanium dioxide, etc. [13-15]. The lifetime test of the DBFC using

0.56%Cu-AEM was carried out to evaluate the stability of Cu-AEMs. As shown in Fig. 7f, the cell has been discharged at 30 °C for over 200 h with a current density of 50 mA·cm^{-1}. The final voltage of the cell is 0.70 V, and the degradation rate is as low as ~0.07% per hour. These results demonstrate that the Cu-AEMs possess both excellent electrochemical properties and stability. The protection of hydrophobic skeletons to $Cu(OH)_2$ nanoclusters explains the unexpected durability of Cu-AEMs.

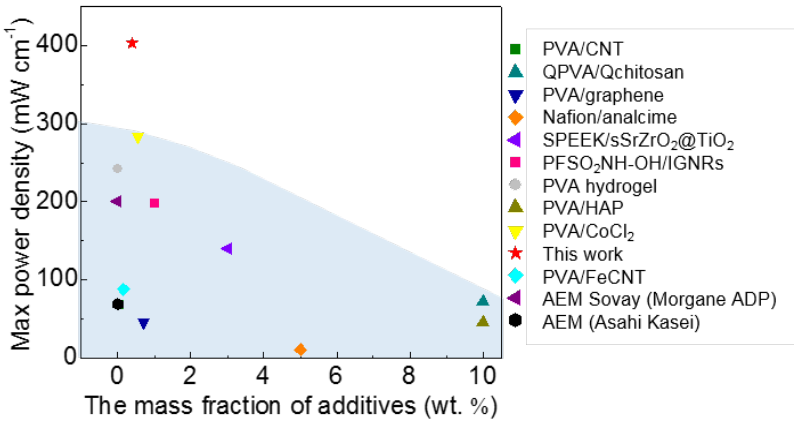

Fig. 8. The P_{max} of recent DBFCs, DMFCs, DAFCs, and AEMFCs using composite AEMs.

Note: DAFCs: direct alcohol fuel cells; DMFCs: direct methanol fuel cells;

AEMFCs: anion exchange membrane hydrogen-oxygen fuel cells

Table 1. The testing conditions of published similar fuel cells with composite AEMs in Fig. 8.

Membranes	**Cells**	**Additives (wt. %)**	**P_{max} (mW·cm^{-2})**	**Catalysts ' C: Cathode catalyst A: Anode catalyst**	**Ref.**
PVA/FeCNT	DMFC	0.15	87.8 (60 °C)	/	[27]
PVA/CNT	DMFC	0.05	68.1 (60 °C)	/	[62]
QPVA/Qchitosan	DAFC	10	73 (60 °C)	C: 6 mg·cm^{-2} PtRu/C; A: 5 mg·cm^{-2} Pt/C	[17]
PVA/graphene	DMFC	0.7	45.8 (60 °C)	5 mg·cm^{-2} 30% Pt	[63]
Nafion/analcime	DMFC	5	10.75	C: 0.5 mg cm^{-2}; A: 2 mg cm^{-2} Pt-Ru/C	[64]
SPEEK/strontium zirconite/TiO_2	DMFC	3	140 (80 °C)	/	[65]
PFSO$_2$NH-OH/ IGNRS	AEMFC	1	197.2 (80 °C)	IGNRs/Pt	[66]
PVA/HAP	DBFC	10	45	/	[67]

PVA/$CoCl_2$	DBFC	0.56	283 (60 °C)	5 mg·cm^{-2} Co-PPy	[29]
PVA/$CuCl_2$	DBFC	0.56	403.3 (60 °C)	5 mg·cm^{-2} Co-PPy	This work
AEM (Asahi Kasei Corporation)	DBFC	/	68.96 (25 °C)	C: 1 mg·cm^{-2} Pt; A: 10 mg cm^{-2} Composites	[68]
AEM Solvay (Morgane® ADP)	DBFC	/	200 (25 °C)	1.3 mg·cm^{-2} Pt	[68]

The P_{max} of the DBFC and the additive content of Cu-AEMs are compared with that of similar published fuel cell systems in Fig. 8. The testing condition of all the fuel cell systems in Fig. 8 are summarized in Table 1. As shown in Fig. 8, the DBFC employing 0.56%Cu-AEM has both a relatively low content of additive and high cell performance. Improving performance significantly with the lowest additive is the everlasting pursuit of nanocomposite researchers. Despite the published CuO nanocomposite, this is the first time that $Cu(OH)_2$ is used to prepare high-performance and stable nanocomposite AEMs [47, 48]. The preparation of simple and eco-friendly $Cu(OH)_2$ nanocomposites is different from the normal 'blending' and can be used to prepare a series of nanocomposites.

3.7. The dominant mechanism of the enhanced Cu-AEMs

There have been many inconsistent views on the functioning mechanism of the nano-additives in nanocomposites. Some studies suggest that the nano-additives hinder the penetration of fuel or accelerated anionic conduction and then improve the properties [69]. Others believe the ratio of conductivity to permeability is the key to the high-performance of nanocomposite AEMs [7, 8, 40]. Since both the fuel and hydroxide ions are anions, the dilemma of conductivity and permeability in DBFCs seems more challenging to resolve. "Hopping" and "vehicle" are two classic theories of ionic conduction in electrolytes, in which ions are hopping along with conductive sites and flowing with solvent, respectively [70, 71]. In this work, the large surface area of dispersive $Cu(OH)_2$ nanoclusters in 0.56%Cu-AEM is beneficial for anionic conducting to "hopping" through [40]. Besides, the nanogaps between PVA and $Cu(OH)_2$ nanoclusters and the outwarded hydroxyl group chains around $Cu(OH)_2$ help expand anionic channels, making the conduction of anions through "vehicle" theory

easier [39, 71, 72]. The decrease of crystallinities and the enlargement of anionic channels in AEMs with $Cu(OH)_2$ nanoclusters are confirmed by the DSC and SAXS results, respectively. Besides, the higher permeability of 0.56%Cu-AEM than blank Cu-AEM results from the accelerated "flowing" instead of "hopping" of BH_4^-, since the $Cu(OH)_2$ nanoclusters prefer to conduct OH^- rather than BH_4^-. The change trends of swell degree, anionic conductivity, and permeability of Cu-AEMs are very similar to each other, reflecting the leading role of "vehicle" theory in the nano-additive modified AEMs for DBFCs.

The 0.56%Cu-AEM has both the highest permeability and performance, since the electric field influence both the movement of OH^- and BH_4^- [44]. A schematic diagram of an operating DBFC with the directions of fuel permeation (*P*, red arrow), hydroxide conduction (*C*, blue arrow), and electric field inside the cell (*E*, black arrow) is shown in the supplementary as Fig. S3. The OH^- conduction from cathode to anode is accelerated while the permeation of the BH_4^- from anode to cathode is hindered by the electric field inside the cell. For OH^-, the electric field promotes both the conduction through "hopping" and "vehicle" mechanisms. For BH_4^-, the electric field is a big obstacle for flowing BH_4^- but has little impact on BH_4^- around conducting sites. The fuel permeation in DBFCs using Cu-AEMs is not very heavy despite its high value. It reflects the importance of anionic conductivity and "vehicle" theory in the improvement of AEMs. Similar results have been published in anionic conduction modeling, which suggests that OH^- are surrounded with two-layer water shells, and the more water content a cell contained, the better mobility the hydroxide ion performed [72].

4. Conclusions

The PVA-based $Cu(OH)_2$ nanocomposite AEMs with excellent performance and stability were prepared by a doping-casting-immersing three-step method for the first time. The chelation property of Cu^{2+} in the PVA matrix and different bonding strength between Cu^{2+} and other components (i.e., PVA, AER, and OH^-) resulted in the even distribution of $Cu(OH)_2$ nanoclusters in Cu-AEMs. The anionic conductivity, fuel permeability, impedances, and cell performance of Cu-AEMs increased when $CuCl_2$ content increased from 0 to 0.56 wt. % but declines at 1.4 wt. %. Different from conventional composites, the swelling degree of Cu-AEMs increased for the separate

hydrophilic and hydrophobic regions in membranes. The improved anionic conductivities result from the unique $Cu(OH)_2$-PVA complex, which enlarges and increases anionic channels in Cu-AEMs. The DBFC employing 0.56%Cu-AEM reached a maximum power density of 403.3 $mW \cdot cm^{-2}$ (60 ^oC) and had a duration of over 200 h. The electric field inside the cell hinders the penetration of fuel and accelerates the conduction of OH^-. The stable $Cu(OH)_2$ -PVA complex is beneficial to extend the duration of Cu-AEMs. 'Vehicle' theory and resulting good anionic conduction are dominant mechanisms of high-performance nanocomposite AEMs for DBFCs. The synthetic chemistry involved in Cu-AEMs could extend for fabricating versatile AEMs with low price, simple preparation, excellent performance, and durability by simply doping Fe^{3+}, Ni^{3+}, Cr^{3+}, etc. into alcoholic polymers.

Acknowledgment

This work is financially supported by the Zhejiang Provincial Natural Science Foundation of China (No. LY18B060005 and LR14B060002), the Natural Science Foundation of Shanghai (17ZR1436800) and the Natural Science Foundation of China (51577166). This research used the Hard X-ray Nanoprobe Beamline at 3-ID of the National Synchrotron Light Source II, a U.S. Department of Energy (DOE) Office of Science User Facility operated for the DOE Office of Science by Brookhaven National Laboratory under Contract No. DE-SC0012704.

Reference:

[1] B. Dunn, H. Kamath, J.M. Tarascon, Electrical energy storage for the grid: a battery of choices. Science 334 (2011) 928-935. doi: 10.1126/science.1212741.

[2] L. Li, Z. Wu, S. Yuan, X.B. Zhang, Advances and challenges for flexible energy storage and conversion devices and systems. Energ. Environ. Sci. 7 (2014) 2101. doi: 10.1039/c4ee00318g.

[3] C.P. de Leon, F.C. Walsh, D. Pletcher, D.J. Browning, J.B. Lakeman, Direct borohydride fuel cells. J. Power Sources 155 (2006) 172-181. doi: 10.1016/j.jpowsour.2006.01.011.

[4] J. Ma, N.A. Choudhury, Y. Sahai, A comprehensive review of direct borohydride fuel cells. Renew. Sust. Energ. Rev. 14 (2010) 183-199. doi: 10.1016/j.rser.2009.08.002.

[5] U.B. Demirci, Direct borohydride fuel cell: Main issues met by the membrane-electrodes-assembly and potential solutions. J. Power Sources 172 (2007) 676-687. doi: 10.1016/j.jpowsour.2007.05.009.

[6] C.G. Arges, L. Zhang, Anion exchange membranes' evolution toward high hydroxide ion conductivity and alkaline resiliency. ACS Appl. Energ. Mater. 1 (2018) 2991-3012. doi:

10.1021/acsaem.8b00387.
[7] H.W. Zhang, P.K. Shen, Recent development of polymer electrolyte membranes for fuel cells. Chem. Rev. 112 (2012) 2780-2832, doi: 10.1021/cr200035s.
[8] S. Kim, S. Jang, S.M. Kim, C.Y. Ahn, W. Hwang, Y.H. Cho, Y.E. Sung, M. Choi, Reduction of methanol crossover by thin cracked metal barriers at the interface between membrane and electrode in direct methanol fuel cells. J. Power Sources 363 (2017) 153-160. doi: 10.1016/j.jpowsour.2017.07.071.
[9] J. Cheng, G. He, F. Zhang, A mini-review on anion exchange membranes for fuel cell applications: Stability issue and addressing strategies. Int. J. Hydrogen Energ. 40 (2015) 7348-7360. doi: 10.1016/j.ijhydene.2015.04.040.
[10] D.J. Kim, M.J. Jo, S.Y. Nam, A review of polymer–nanocomposite electrolyte membranes for fuel cell application. J. Ind. Eng. Chem. 21 (2015) 36-52. doi: 10.1016/j.jiec.2014.04.030.
[11] B.P. Tripathi, V.K. Shahi, Organic–inorganic nanocomposite polymer electrolyte membranes for fuel cell applications. Prog. Polym. Sci. 36 (2011) 945-979. doi: 10.1016/j.progpolymsci.2010.12.005.
[12] X. Li, J. Tao, G. Nie, L. Wang, L. Li, S. Liao, Cross-linked multiblock copoly(arylene ether sulfone) ionomer/nano-ZrO_2 composite anion exchange membranes for alkaline fuel cells. RSC Adv. 4 (2014) 41398-41410. doi: 10.1039/c4ra06519k.
[13] X. Li, Y. Yu, Y. Meng, Novel quaternized poly(arylene ether sulfone)/Nano-ZrO(2) composite anion exchange membranes for alkaline fuel cells. ACS Appl. Mater. Interfaces 5 (2013) 1414-1422. doi: 10.1021/am302844x.
[14] M.T. Taghizadeh, M. Vatanparast, Preparation and evaluation of Nafion/SnO_2 nanocomposite for improving the chemical durability of proton exchange membranes in fuel cells. RSC Adv. 6 (2016) 56819-56826. doi: 10.1039/c6ra07849d.
[15] W.F. Chan, H.C.A. Surapathi, M.G. Taylor, X. Shao, E. Marand, J.K. Johnson, Zwitterion Functionalized Carbon Nanotube/Polyamide Nanocomposite Membranes for Water Desalination. ACS Nano 7 (2013) 5308-5319. doi: 10.1021/nn4011494
[16] J.S. Lin, S.R. Kumar, W.T. Ma, C.M. Shih, L.W. Teng, C.C. Yang, S.J. Lue, Gradiently distributed iron oxide@graphene oxide nanofillers in quaternized polyvinyl alcohol composite to enhance alkaline fuel cell power density. J. Membrane Sci. 543 (2017) 28-39. doi: 10.1016/j.memsci.2017.08.045.
[17] G.M. Liao, C.C. Yang, C.C. Hu, Y.L. Pai, S.J. Lue, Novel quaternized polyvinyl alcohol/quaternized chitosan nano-composite as an effective hydroxide-conducting electrolyte. J. Membrane Sci. 485 (2015) 17-29, doi: 10.1016/j.memsci.2015.02.043.
[18] B. Gilbert, R.K. Ono, K.A. Ching, C.S. Kim, The effects of nanoparticle aggregation processes on aggregate structure and metal uptake. J. Colloid. Interface Sci. 339 (2009) 285-295. doi: 10.1016/j.jcis.2009.07.058.
[19] L.Y. Yu, H.M. Shen, Z.L. Xu, PVDF-TiO_2 composite hollow fiber ultrafiltration membranes

prepared by TiO_2 sol-gel method and blending method. J. Appl. Polym. Sci. 113 (2009) 1763-1772. doi: 10.1002/app.29886.
[20] H. Vinh-Thang, S. Kaliaguine, Predictive models for mixed-matrix membrane performance: a review. Chem. Rev. 113 (2013) 4980-5028. doi: 10.1021/cr3003888.
[21] J.F. Wu, C.F. Lo, L.Y. Li, H.Y. Li, C.M. Chang, K.S. Liao, C.C. Hu, Y.L. Liu, S.J. Lue, Thermally stable polybenzimidazole/carbon nano-tube composites for alkaline direct methanol fuel cell applications. J. Power Sources 246 (2014) 39-48. doi: 10.1016/j.jpowsour.2013.05.171.
[22] H.C. Yang, J. Hou, V. Chen, Z.K. Xu, Surface and interface engineering for organic–inorganic composite membranes. J. Mater. Chem. A 4 (2016) 9716-9729. doi: 10.1039/c6ta02844f.
[23] L.Y. Ng, A.W. Mohammad, C.P. Leo, N. Hilal, Polymeric membranes incorporated with metal/metal oxide nanoparticles: A comprehensive review. Desalination 308 (2013) 15-33. doi: 10.1016/j.desal.2010.11.033.
[24] Y. Xiong, Q.L. Liu, A.M. Zhu, S.M. Huang, Q.H. Zeng, Performance of organic–inorganic hybrid anion-exchange membranes for alkaline direct methanol fuel cells. J. Power Sources 186 (2009) 328-333. doi: 10.1016/j.jpowsour.2008.10.070.
[25] M. Miculescu, V.K. Thakur, F. Miculescu, S.I. Voicu, Graphene-based polymer nanocomposite membranes: a review. Polym. Advan. Technol. 27 (2016) 844-859. doi: 10.1002/pat.3751.
[26] G. Rambabu, D.B. Santoshkumar, F.M.L. Figueiredo, Carbon Nanocomposite Membrane Electrolytes for Direct Methanol Fuel Cells-A Concise Review. Nanomaterials 9 (2019) 1292. doi: 10.3390/nano9091292.
[27] C.F. Lo, J.F. Wu, H.Y. Li, W.S. Hung, C.M. Shih, C.C. Hu, Y.L. Liu, S.J. Lue, Novel polyvinyl alcohol nanocomposites containing carbon nano-tubes with Fe3O4 pendants for alkaline fuel cell applications. J. Membrane Sci. 444 (2013) 41-49. doi: 10.1016/j.memsci.2013.05.001.
[28] B. Kaker, S. Hribernik, T. Mohan, R. Kargl, K.S. Kleinschek, E. Pavlica, A. Kreta, G. Bratina, S. J. Lue, M. Božič, Novel Chitosan-$Mg(OH)_2$-Based Nanocomposite Membranes for Direct Alkaline Ethanol Fuel Cells. ACS Sustain. Chem. Eng. 7 (2019) 19356-19368, doi:10.1021/acssuschemeng.9b02888.
[29] H. Qin, L. Lin, W. Chu, W. Jiang, Y. He, Q. Shi, Y. Deng, Z. Ji, J. Liu, S. Tao, Introducing catalyst in alkaline membrane for improved performance direct borohydride fuel cells. J. Power Sources 374 (2018) 113-120. doi: 10.1016/j.jpowsour.2017.11.008.
[30] F.J. Fan, Y.J. Zhan, J.H. Zhu, J.M. Song, S.H. Yu, Fluorescent bracelet-like Cu@cross-linked poly(vinyl alcohol) (PVA) microrings by a hydrothermal process. RSC Adv. 1 (2011) 67-72. doi: 10.1039/C1RA00227A.
[31] Z. Li, H. Huang, C. Wang. Electrostatic Forces Induce Poly(vinyl alcohol)-Protected Copper Nanoparticles to Form Copper/Poly(vinyl alcohol) Nanocables via Electrospinning. Macromol. Rapid Comm. 27 (2006) 152-155. doi: 10.1002/marc.200500627.

[32] J. Yu, J. Ran, Facile preparation and enhanced photocatalytic H_2-production activity of $Cu(OH)_2$ cluster modified TiO_2. Energ. Environ. Sci. 4 (2011) 1364. doi: 10.1039/c0ee00729c.
[33] S.K. Shinde, D.P. Dubal, G.S. Ghodake, D.Y. Kim, V.J. Fulari, Nanoflower-like CuO/Cu(OH)2 hybrid thin films: Synthesis and electrochemical supercapacitive properties. J. Electroanal. Chem. 732 (2014) 80-85. doi: 10.1016/j.jelechem.2014.09.004.
[34] G. Couture, A. Alaaeddine, F. Boschet, B. Ameduri, Polymeric materials as anion-exchange membranes for alkaline fuel cells. Prog. Polym. Sci. 36 (2011) 1521-1557. doi: 10.1016/j.progpolymsci.2011.04.004.
[35] O. Akhavan, R. Azimirad, S. Safa, E. Hasani, $CuO/Cu(OH)_2$ hierarchical nanostructures as bactericidal photocatalysts. J. Mater. Chem. 21 (2011) 9634. doi: 10.1039/c0jm04364h.
[36] H. Yokoi, S. Kawata, M. Iwaizumi, Interaction modes between heavy metal ions and water-soluble polymers. 1. Spectroscopic and magnetic reexamination of the aqueous-solutions of cupric ions and polyvinyl-alcohol. J. Am. Chem. Soc. 108 (1986) 3358-3361.
[37] Y. Matsuo, K. Hatase, Y. Sugie, Preparation and characterization of Poly(vinyl alcohol) and Cu (OH)2-Poly(vinyl alcohol)-intercalated graphite oxides. Chem. Mater. 10 (1998) 2266-2269. doi: 10.1021/cm980203a.
[38] G.H. Du, G.Van Tendeloo, $Cu(OH)_2$ nanowires, CuO nanowires and CuO nanobelts. Chem. Phys. Lett. 393 (2004) 64-69. doi: 10.1016/j.cplett.2004.06.017.
[39] N.N. Krishnan, D. Henkensmeier, J.H. Jang, H.J. Kim, Nanocomposite Membranes for Polymer Electrolyte Fuel Cells. Macromol. Mater. Eng. 299 (2014) 1031-1041. doi: 10.1002/mame.201300378.
[40] X. Tong, B. Zhang, Y. Fan, Y. Chen, Mechanism Exploration of Ion Transport in Nanocomposite Cation Exchange Membranes. ACS Appl. Mater. Interfaces 9 (2017) 13491-13499. doi: 10.1021/acsami.7b01541.
[41] G. Li, J. Pan, J. Han, C. Chen, J. Lu, L. Zhuang, Ultrathin composite membrane of alkaline polymer electrolyte for fuel cell applications. J. Mater. Chem. A 1 (2013) 12497. doi: 10.1039/c3ta12626a.
[42] Y. Yin, Y. Liu, H. Wu, L. Cao, X. He, B. Zhang, C. Wang, Z. Zhang, One-pot synthesis of silica–titania binary nanoparticles with acid–base pairs via biomimetic mineralization to fabricate highly proton-conductive membranes. J. Mater. Chem. A 5 (2017) 18585-18593. doi: 10.1039/c7ta03513f.
[43] H. Qin, Y. Hu, C. Zhu, W. Chu, H. Sheng, Z. Dong, Y. He, J. Wang, A. Li, H. Chi, H. Ni, Z. Ji, J. Liu, Functionalization of polyvinyl alcohol composite membrane by CoOOH for direct borohydride fuel cells. Electrochem. Commun. 77 (2017) 1-4. doi: 10.1016/j.elecom.2017.02.005.
[44] W. Chu, W. Jiang, H. Sheng, G. Yuan, W. Lin, L. Lin, H. Qin, L. Meng, J. Liu, Fuel permeability of anion exchange membranes under electric field. Electrochimi. Acta 266 (2018) 357-363. doi: 10.1016/j.electacta.2018.01.183.
[45] C. Deng, Q.G. Zhang, G.L. Han, Y. Gong, A.M. Zhu, Q.L. Liu, Ultrathin self-assembled

anionic polymer membranes for superfast size-selective separation. Nanoscale 5 (2013) 11028-11034. doi: 10.1039/c3nr03362g.
[46] Y. Mao, L. shi, H. Huang, W. Cao, J. Li, L. Sun, X. Jin, X. Peng, Room temperature synthesis of free-standing HKUST-1 membranes from copper hydroxide nanostrands for gas separation. Chem. Commun. 49 (2013) 5666-5668. doi: 10.1039/c3cc42601g.
[47] E. Kociołek-Balawejder, E. Stanisławska, I. Jacukowicz-Sobala, Synthesis and characterization of CuO-loaded macroreticular anion exchange hybrid polymer. React. Funct. Polym. 100 (2016) 107-115. doi: 10.1016/j.reactfunctpolym.2016.01.010.
[48] E. Kociołek-Balawejder, E. Stanisławska, I. Jacukowicz-Sobala, D. Ociński, CuO-Loaded Macroreticular Anion Exchange Hybrid Polymers Obtained via Tetrachlorocuprate(II) Ionic Form. Int. J. Polym. Sci. (2017) 1-6. doi: 10.1155/2017/4574397.
[49] M. E. A. Ali, F.M. Hassan, X. Feng, Improving the performance of TFC membranes via chelation and surface reaction: applications in water desalination. J. Mater. Chem. A 4 (2016) 6620-6629. doi: 10.1039/c6ta01460g.
[50] Y.J. Wang, D. Kim, Crystallinity, morphology, mechanical properties and conductivity study of in situ formed PVdF/$LiClO_4$/TiO_2 nanocomposite polymer electrolytes. Electrochimi. Acta 52 (2007) 3181-3189. doi: 10.1016/j.electacta.2006.09.070.
[51] J. Yin, E.S. Kim, J. Yang, B. Deng, Fabrication of a novel thin-film nanocomposite (TFN) membrane containing MCM-41 silica nanoparticles (NPs) for water purification. J. Membrane Sci. 423 (2012) 238-246. doi: 10.1016/j.memsci.2012.08.020.
[52] F. Parvin, M.A. Khan, A.H.M. Saadat, M.A.H. Khan, J.M.M. Islam, M. Ahmed, M.A. Gafur, Preparation and Characterization of Gamma Irradiated Sugar Containing Starch/Poly(vinyl alcohol)-Based Blend Films. J. Polym. Environ. 19 (2011) 1013-1022. doi: 10.1007/s10924-011-0357-6.
[53] J. Zhang, T. Zhou, J. Qiao, Y. Liu, J. Zhang, Hydroxyl anion conducting membranes poly(vinyl alcohol)/poly(diallyldimethylammonium chloride) for alkaline fuel cell applications: Effect of molecular weight. Electrochimi. Acta 111 (2013) 351-358. doi: 10.1016/j.electacta.2013.07.182.
[54] Z. Derbali, A. Fahs, J.F. Chailan, I.V. Ferrari, M.L. Di Vona, P. Knauth, Composite anion exchange membranes with functionalized hydrophilic or hydrophobic titanium dioxide. Int. J. Hydrogen. Energ. 42 (2017) 19178-19189, doi: 10.1016/j.ijhydene.2017.05.208.
[55] X.F. Qian, J. Yin, J.C. Huang, Y.F. Yang, X.X. Guo, Z.K. Zhu, The preparation and characterization of PVA/Ag_2S nanocomposite. Mater. Chem. Phys. 68 (2001) 95-97.
[56] K. Kaneko, A. Kobayashi, T. Suzuki, S. Ozeki, K. Kakei, N. Kosugi, H. Kuroda, The dimer state of no in micropores of $Cu(OH)_2$-dispersed activated carbon-fibers. Journal of the Chemical Society-Faraday Transactions I 84 (1988) 1795-1805. doi: 10.1039/f19888401795.
[57] Y. Yang, F. Lu, X. Gao, S. Xie, N. Sun, L. Zheng, Effect of different ion-aggregating structures on the property of proton conducting membrane based on polyvinyl alcohol. J.

Membrane Sci. 490 (2015) 38-45. doi: 10.1016/j.memsci.2015.04.058.
[58] D.R. Dekel, Review of cell performance in anion exchange membrane fuel cells. J. Power Sources 375 (2018) 158-169. doi: 10.1016/j.jpowsour.2017.07.117.
[59] Z. Zhao, S. Shi, H. Cao, Y. Li, Electrochemical impedance spectroscopy and surface properties characterization of anion exchange membrane fouled by sodium dodecyl sulfate. J. Membrane Sci. 530 (2017) 220-231. doi: 10.1016/j.memsci.2017.02.037.
[60] S. Asghari, A. Mokmeli, M. Samavati, Study of PEM fuel cell performance by electrochemical impedance spectroscopy. Int. J. Hydrogen Energ. 35 (2010) 9283-9290. doi: 10.1016/j.ijhydene.2010.03.069.
[61] S.M. Rezaei Niya, M. Hoorfar, Study of proton exchange membrane fuel cells using electrochemical impedance spectroscopy technique-A review. J. Power Sources 240 (2013) 281-293. doi: 10.1016/j.jpowsour.2013.04.011.
[62] S.J. Lue, W.H. Pan, C.M. Chang, Y.L. Liu, High-performance direct methanol alkaline fuel cells using potassium hydroxide-impregnated polyvinyl alcohol/carbon nano-tube electrolytes. J. Power Sources 202 (2012) 1-10. doi: 10.1016/j.jpowsour.2011.10.091.
[63] Y.S. Ye, M.Y. Cheng, X.L. Xie, J. Rick, Y.J. Huang, F.C. Chang, B.J. Hwang, Alkali doped polyvinyl alcohol/graphene electrolyte for direct methanol alkaline fuel cells. J. Power Sources 239 (2013) 424-432. doi: 10.1016/j.jpowsour.2013.03.021.
[64] P. Prapainainar, Z. Du, P. Kongkachuichay, S.M. Holmes, C. Prapainainar, Mordenite/Nafion and analcime/Nafion composite membranes prepared by spray method for improved direct methanol fuel cell performance. Appl. Surf. Sci. 421 (2017) 24-41. doi: 10.1016/j.apsusc.2017.02.004.
[65] G. Gnana kumar, A. Manthiram, A. Sulfonated polyether ether ketone/strontium zirconite@TiO_2 nanocomposite membranes for direct methanol fuel cells. J. Mater. Chem. A 5 (2017) 20497-20504. doi: 10.1039/c7ta06258c.
[66] X. Liu, X. Cheng, Y. Hu, T. Gong, H. Li, Y. Zhang. Ionic-Liquid-Functionalized Graphene Nanoribbons for Anion Exchange Membrane Fuel Cells. J. Electrochemi. Soc. 164 (2017) 433-440. doi: 10.1149/2.0141706jes].
[67] C.C. Yang, Y.J. Li, S.J. Chiu, K.T. Lee, W.C. Chien, C.A. Huan, A direct borohydride fuel cell based on poly(vinyl alcohol)/hydroxyapatite composite polymer electrolyte membrane. J. Power Sources 184 (2008) 95-98. doi: 10.1016/j.jpowsour.2008.06.042.
[68] H. Qin, Z. Liu, Y. Guo, Z. Li, The affects of membrane on the cell performance when using alkaline borohydride–hydrazine solutions as the fuel. Int. J. Hydrogen Energ. 35 (2010) 2868-2871. doi: 10.1016/j.ijhydene.2009.05.004.
[69] Y. Chen, S. Zhang, J. Jin, C. Liu, Q. Liu, X. Jian, Poly(phthalazinone ether ketone) Amphoteric Ion Exchange Membranes with Low Water Transport and Vanadium Permeability for Vanadium Redox Flow Battery Application. ACS Appl. Energ. Mater. 2 (2019) 8207-8218. doi: 10.1021/acsaem.9b01687.

[70] Y.Z. Fu, A. Manthiram, Synthesis and characterization of sulfonated polysulfone membranes for direct methanol fuel cells. J. Power Sources 157 (2006) 222-225. doi: 10.1016/j.jpowsour.2005.08.007.
[71] J. Shen, J. Xi, W. Zhu, L. Chen, X. Qiu, A nanocomposite proton exchange membrane based on PVDF, poly(2-acrylamido-2-methyl propylene sulfonic acid), and nano-Al_2O_3 for direct methanol fuel cells. J. Power Sources 159 (2006) 894-899. doi: 10.1016/j.jpowsour.2005.11.070.
[72] C. Wang, B. Mo, Z. He, X. Xie, C.X. Zhao, L. Zhang, Q. Shao, X. Guo, E.K. Wujcik, Z. Guo, Hydroxide ions transportation in polynorbornene anion exchange membrane. Polymer 138 (2018) 363-368. doi: https://doi.org/10.1016/j.polymer.2018.01.079.